

# Evaluation of the influence of El Niño–Southern Oscillation on air quality in southern China from long-term historical observations

Shansi Wang<sup>1</sup>, Siwei Li (✉)<sup>1,2</sup>, Jia Xing<sup>3</sup>, Jie Yang<sup>2</sup>, Jiaxin Dong<sup>1</sup>, Yu Qin<sup>4</sup>, Shovan Kumar Sahu<sup>3</sup>

<sup>1</sup> School of Remote Sensing and Information Engineering, Wuhan University, Wuhan 430079, China

<sup>2</sup> State Key Laboratory of Information Engineering in Surveying, Mapping and Remote Sensing, Wuhan University, Wuhan 430079, China

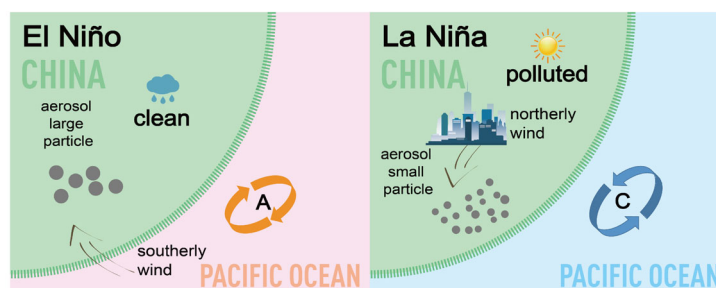
<sup>3</sup> School of Environment, Tsinghua University, Beijing 100084, China

<sup>4</sup> Map Institute of Guangdong Province, Guangzhou 510075, China

## HIGHLIGHTS

- Strong ENSO influence on AOD is found in southern China region.
- Low AOD occurs in El Niño but high AOD occurs in La Niña events in southern China.
- Angstrom exponent anomalies reveals the circulation pattern during each ENSO phase.
- ENSO exerts large influence (70.5%) on annual variations of AOD during 2002–2020.
- Change of anthropogenic emissions is the dominant driver for AOD trend (2002–2020).

## GRAPHIC ABSTRACT



## ARTICLE INFO

### Article history:

Received 7 March 2021

Revised 20 April 2021

Accepted 6 May 2021

Available online 11 June 2021

### Keywords:

El Niño–Southern Oscillation  
Aerosol concentration  
Aerosol particle size  
Contribution separation  
Decadal trend  
Southern China

## ABSTRACT

Previous studies demonstrated that the El Niño–Southern Oscillation (ENSO) could modulate regional climate thus influencing air quality in the low-middle latitude regions like southern China. However, such influence has not been well evaluated at a long-term historical scale. To filling the gap, this study investigated two-decade (2002 to 2020) aerosol concentration and particle size in southern China during the whole dynamic development of ENSO phases. Results suggest strong positive correlations between aerosol optical depth (AOD) and ENSO phases, as low AOD occurred during El Niño while high AOD occurred during La Niña event. Such correlations are mainly attributed to the variation of atmospheric circulation and precipitation during corresponding ENSO phase. Analysis of the angstrom exponent (AE) anomalies further confirmed the circulation pattern, as negative AE anomalies is pronounced in El Niño indicating the enhanced transport of sea salt aerosols from the South China Sea, while the La Niña event exhibits positive AE anomalies which can be attributed to the enhanced import of northern fine anthropogenic aerosols. This study further quantified the AOD variation attributed to changes in ENSO phases and anthropogenic emissions. Results suggest that the long-term AOD variation from 2002 to 2020 in southern China is mostly driven (by 64.2%) by the change of anthropogenic emissions from 2002 to 2020. However, the ENSO presents dominant influence (70.5%) on year-to-year variations of AOD during 2002–2020, implying the importance of ENSO on varying aerosol concentration in a short-term period.

© Higher Education Press 2022

## 1 Introduction

Along with rapid economic development in recent decades, China is facing serious problem of air pollution

which is harmful to human health (Jiang et al., 2021) and climate change (Koren et al., 2012). In addition to high annual averaged pollution level, extreme haze pollution events have also occurred frequently in recent years (Zhang et al., 2014; Yin et al., 2017) which is considered to be mostly contributed by the unfavorable meteorological conditions (Liu et al., 2017) and climatic deterioration resulting in decreased large scale atmospheric circulation

✉ Corresponding author

E-mail: siwei.li@whu.edu.cn

(Zhu et al., 2012; Ding et al., 2017). For instance, Zhao et al. (2016) indicated that intensified positive Pacific Decadal Oscillation (PDO) could result in stable stratification of the atmosphere and consequent wintertime haze in central eastern China. Cai et al. (2017) found that the upward trend of Arctic Oscillation (AO) conduces to Beijing severe haze. Some studies also revealed that the declining of Autumn Arctic Sea accounted for the increase in winter haze days (Zou et al., 2017).

As the control of anthropogenic emissions has been continually strengthened since 2013 in China with the enforcement of Air Pollution Prevention and Control Action Plan (note as Action Plan) (Ding et al., 2019a; Shang et al., 2021), the impact of meteorological variation on air quality gains more and more attention. For example, Ma et al. (2019) indicated that daily changes of pollutant concentrations in Yangtze River Delta (YRD) were mainly controlled by meteorological conditions. Ding et al. (2019b) revealed that ozone pollution in China is largely influenced by emission as well as meteorological factors. Moreover, the variation of large-scale circulation is expected to be driven by future climate change, which may largely influence the air quality. Previous studies suggest that the El Niño-Southern Oscillation (noted as ENSO), which is also the biggest cause of large-scale climate variability in the tropics, produces anomalous atmospheric circulation and exerts significant impacts on climate of low-middle latitude through teleconnection (Wang et al., 2000), and consequently influences the air quality. For example, Chang et al. (2016) found that 2015 strong El Niño resulted in severe air pollution in North China Plain (NCP) as well as in eastern China. Sun et al. (2018) suggested that ENSO led to more influences over southern China. Wang et al. (2019) revealed that recent ENSO including El Niño (2015/2016) and the following La Niña events (2017/2018), resulted in higher PM<sub>2.5</sub> concentration in northern China while low PM<sub>2.5</sub> pollution prevailed in southern China during El Niño period. Feng et al. (2016) found that 1994/1995 El Niño Modoki played a leading role in aerosol concentrations over southern China due to a rise in concentration (~30%) compared with the climatological mean value. Feng et al. (2017) also revealed increased aerosol concentrations in the southern China during 1998/1999 La Niña Modoki mature phase while reduced aerosol concentration during 2000/2001. However, uncertainties of ENSO influence remain in current research findings. Furthermore, most of previous studies investigated the ENSO impacts on northern China Plain (NCP) (Zhang et al., 2019). Compared to NCP, southern China is even closer to the tropical Pacific thus may suffer stronger influences from ENSO (Chen et al., 2014), while relevant studies about ENSO influence on southern China region are also quite limited.

More importantly, analyzing decadal trend of the ENSO influence on air quality based on long-term observation data could be of much help for better understanding the

potential increasing frequency of extreme ENSO stemming from greenhouse warming (Capotondi, 2015; Cai et al., 2018) which becomes a challenge to further improve the air quality in China. Additionally, it is also important to understand the relative contributions to air quality from natural ENSO fluctuation and anthropogenic emissions, as strengthened air pollution control is ongoing in China.

This paper aims to investigate the impact of different ENSO development phases (from autumn developing phase to winter mature to spring decaying phase) on the spatio-temporal distribution of aerosol over southern China. The relative contributions of ENSO and emission changes to AOD variations were quantified based on long-term historical observations.

The rest paper is organized as follows: Section 2 briefly introduces research data and methodology. Section 3 illustrates the various features of aerosol optical depth (AOD) and angstrom exponent (AE) during different ENSO development phases. Section 4 explains the potential influence mechanisms from atmospheric circulation of ENSO events on aerosols. Section 5 further discusses the model results and relative contributions to air quality from natural ENSO fluctuation and anthropogenic emissions. Section 6 is the conclusion.

---

## 2 Data and method

The study area encompasses the south of mainland China (105.5°–122°E, 20.5°–34°N), which is located on the third and lowest ladder of China. Southern region is roughly in non-heating area, which lies to the south of the boundary of the Huai River and Qinling Mountains.

### 2.1 Data

#### 2.1.1 Oceanic Niño Index (ONI)

Three month running mean sea surface temperature anomaly (SSTA) in the Niño 3.4 region (5°N–5°S, 120–170°W) is defined as ONI to represent different ENSO development phases. The ONI was obtained from the Climate Prediction Center (CPC) of the National Oceanic and Atmospheric Administration (NOAA) (the homepage of NOAA).

#### 2.1.2 AOD

We used monthly AOD product retrieval at 550 nm based on Deep Blue algorithms from Moderate Resolution Imaging Spectroradiometer (MODIS) on Aqua's satellite at a 1° × 1° horizontal resolution. The quality of MODIS AOD data has been evaluated in previous applications (Kim et al., 2007) which demonstrate that the AOD products can well capture the features of spatio-temporal

distribution of aerosol over China. It is noteworthy that MODIS AOD product is preferred considering its widespread application and high quality compared with other satellite products that is not suitable for this study, because either the time or the scope are a mismatch. For example, some instruments provide aerosol products before 2000, like Advanced Very High Resolution Radiometer (AVHRR) from NOAA, but it is observation only cover ocean. On the other hand, Modern-Era Retrospective analysis for Research and Applications, Version 2 (MERRA-2) provides data beginning in 1980. However, unlike direct observation from satellite instrument, MERRA-2 is the product of model assimilation after 1999. More importantly, performance of MERRA2 over China has rarely been evaluated in previous studies. So, MODIS instrument is still the best choice for this study.

### 2.1.3 Climate variables

The atmospheric circulation data from ERA5 monthly reanalysis climate data set provided by the European Centre for Medium-Range Weather Forecasts (ECMWF), including monthly total precipitation, surface wind vector, 850-hPa wind vector, 500-hPa wind vector, 500-hPa geopotential height (hgt500), and surface relative humidity is used in this study. Here, we selected 850 and 500-hPa levels because both of them are the typical height of the lower and middle troposphere, to represent the surface and upper-air circulation patterns, respectively. Previous studies show that the near-surface wind speed provided in ERA5 agrees well with the situ observation (Ramon et al., 2019).

All data used are monthly averaged over a time span from September 2002 to May 2020 to match time of available AOD product. The climatological-mean value was calculated as the corresponding monthly mean from 2002 to 2020, and anomaly value was also used for each month by removing climatological-mean state (Fig. 1). The

ONI exhibits great fluctuations across the study period, especially in the super ENSO events such as 2009/2010, 2015/2016 super El Niño, 2007/2008 and 2010/2011 super La Niña. ONI can robustly show consistent features during these three super El Niño during 1982/1983, 1997/1998, 2015/2016 (Fig. S1).

ENSO composites include developing period, peak period and decaying periods. In this study, ENSO developing period is defined as three months in autumn during September–October–November (SON). ENSO peak period refers to three months in winter during December–January–February (DJF), and ENSO decaying period refers to three months in spring from March, April to May (MAM). In this study, 54 SON months, 54 months DJF and 54 MAM months were taken into consideration, corresponding to ENSO developing period, peak period and decaying period during 2002–2020, respectively. We further divided those months into El Niño and La Niña months according to NOAA-CPC, as summarized in Table 1. ENSO winter (DJF) events are shown as Table S1.

**Table 1** ENSO development phase and events division during 2002–2020

Name	El Niño	La Niña	Neutral
Developing (SON)	19	16	19
Peak (DJF)	23	19	12
Decaying (MAM)	11	10	33

## 2.2 Methods

### 2.2.1 Anthropogenic emission changes and associated impacts on aerosols

The ABaCAS (Air Benefit and Cost and Attainment Assessment System) provides the long-term emission inventory (ABaCAS-EI) in China developed by Tsinghua

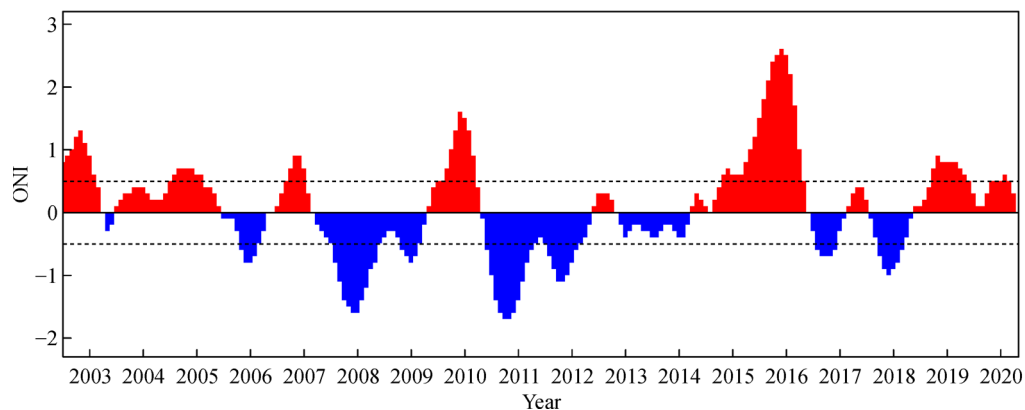


**Fig. 1** The ONI during ENSO development from 2002 to 2020 (unit: °C) (Above 0.5°C is defined as an El Niño event, below −0.5°C is defined as a La Niña event, between −0.5°C and 0.5°C is defined as a neutral event).

University (<http://abacas.see.scut.edu.cn/abacas/Default.aspx>) (Xing et al., 2020a). Historical trend of anthropogenic emissions of five major pollutants in southern China is shown in Fig. 2. The response surface model (RSM) in ABaCAS also provides real-time estimates of air quality response to the change of major pollutants including  $\text{NO}_x$ ,  $\text{SO}_2$ ,  $\text{NH}_3$ , volatile organic compounds (VOC) and primary  $\text{PM}_{2.5}$ . The  $\text{PM}_{2.5}$  concentrations under each year of emission levels with fixed meteorology condition (noted as emission index) were estimated by RSM to represent the overall impacts on aerosols due to the emission change of five pollutants (Xing et al., 2020b). A sharply decline trend of  $\text{NO}_x$  and  $\text{SO}_2$  as well as  $\text{PM}_{2.5}$  occurred after 2013 and 2005 respectively (see Fig. 2). The overall trend of RSM-predicted  $\text{PM}_{2.5}$  concentrations (i.e., emission index) also decreased since 2013, even though under limited controls on VOC and  $\text{NH}_3$ .

A similar normalization processing to ENSO index has

been conducted on the emission index, by which the emission index is analyzed by anomalies during 2002–2020 (as shown in Fig. 3). Emission index increases at initial period and then declined gradually, while AOD decreases particularly after 2013 when the Chinese government introduced the “Action Plan” in 2013 (Ding et al., 2019a) to effectively control anthropogenic emissions.

### 2.2.2 Quantification of relative impacts of ENSO on AOD variations

The long-term observations provide a unique opportunity to quantify the relative impacts of ENSO on AOD variations. In this study, we use the Multiple Linear Regression (MLR), which is a mature approach (Tai et al., 2010; Wu et al., 2019) to separate the individual effect of anthropogenic emissions and natural ENSO fluctuation on

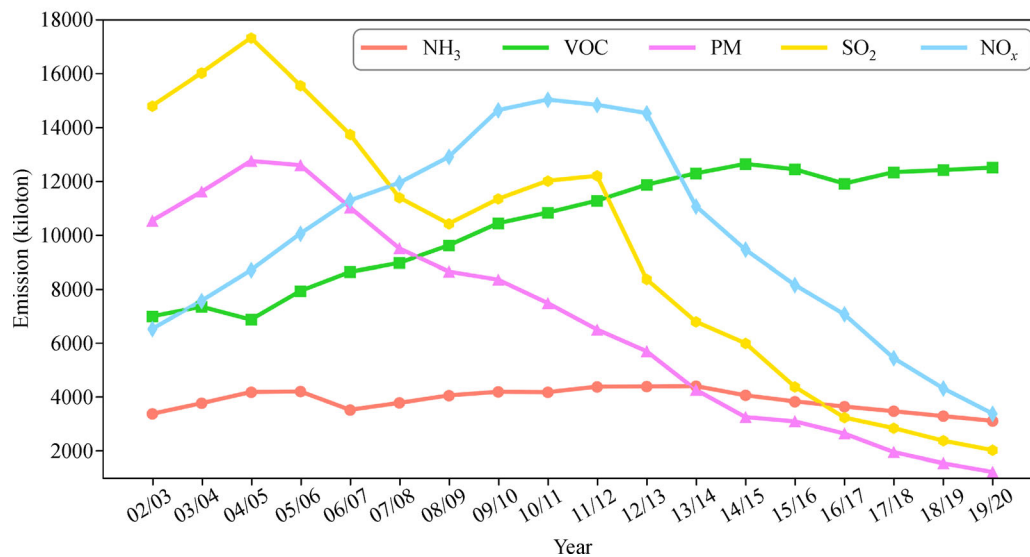


**Fig. 2** Historical trend of anthropogenic emissions of five major pollutants in southern China.

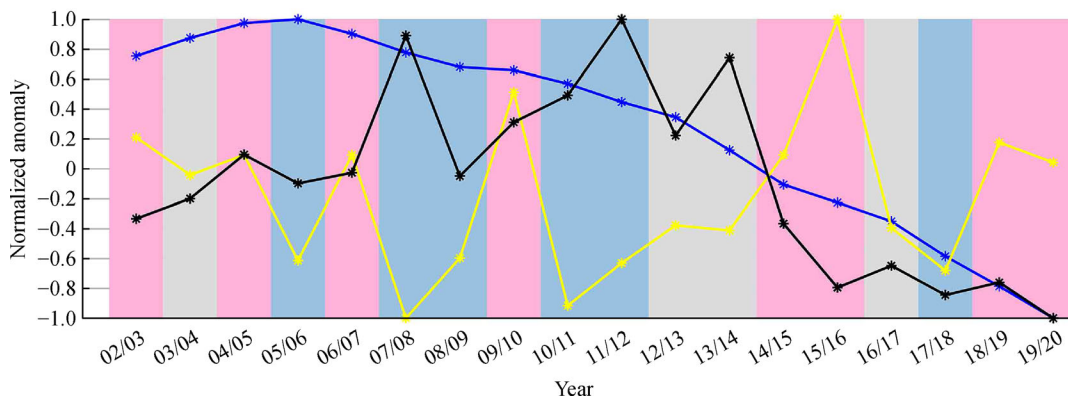


**Fig. 3** The time series of peak winter (DJF) anomaly of AOD (black), ONI (yellow) and emission index (blue) (all are processed as standardization data ranged from  $-1$  to  $1$  interval).

PM<sub>2.5</sub> (or AOD) variability. Details can be found as follows.

$$\Delta AOD = \beta_1 \Delta x_1 + \beta_2 \Delta x_2 + b, \quad (1)$$

where AOD is the anomaly AOD values, the two independent variables are the change of emission index (noted as  $\Delta x_1$ ) and the change of ENSO index (noted as  $\Delta x_2$ ).  $\beta_1$  and  $\beta_2$  represent the coefficient of emissions and ENSO respectively.  $b$  represents intercept term.

Here, it should be noted that we use ENSO index (ONI) to characterize natural meteorological factors rather than individual parameters such as local precipitation, wind speed or relative humidity. The reason is that ENSO is an ocean-atmosphere coupling phenomenon and thus would require several meteorological parameters to fully represent its total influence, though precipitation and wind field is relatively more important (analyzed in detail in Section 4). Actually, the ENSO index and local meteorological conditions agree well with strong correlation coefficient (0.74, see Fig. S2 which presents the correlations between ONI and precipitation), indicating that the ONI can reflect the local meteorological parameters. Therefore, the ONI was used instead of local parameters to estimate the impact of ENSO.

Next, we quantify the relative contribution of ENSO and emission changes based on the results of MLR model, as follows.

First, we calculate the annual contribution of emission and ENSO, as described in the Eqs. (2) and (3). Here, there are 18 winters from 2002 to 2020 (2019 winter), so index  $i$  is years from 1 to 18, and the same  $i$  in the following formula.

$$Emission_{(i)} = \frac{\beta_1 x_{1(i)}}{\beta_1 x_{1(i)} + \beta_2 x_{2(i)}} * 100\%, \quad (2)$$

$$ENSO_{(i)} = \frac{\beta_2 x_{2(i)}}{\beta_1 x_{1(i)} + \beta_2 x_{2(i)}} * 100\%. \quad (3)$$

Then long-term impacts of anthropogenic emissions and ENSO events were averaged in the 18 years based on Eqs. (4) and (5), as follows.

$$Contribution_{Emission} = \frac{\sum_{i=1}^{18} Emission_{(i)}}{18}, \quad (4)$$

$$Contribution_{ENSO} = \frac{\sum_{i=1}^{18} ENSO_{(i)}}{18}. \quad (5)$$

The annual contribution of emission and ENSO calculated in Eqs. (2) and (3) can be positive or negative in short-term (annual). To eliminate the influence of counteract of positive and negative values, we additionally

estimate the relative contribution of ENSO and emission changes on decadal scale based on Eqs. (6) and (7), as follows.

$$Emission_{(i)} = \frac{|\beta_1 \Delta x_{1(i)}|}{|\beta_1 \Delta x_{1(i)}| + |\beta_2 \Delta x_{2(i)}|} * 100\%, \quad (6)$$

$$ENSO_{(i)} = \frac{|\beta_2 \Delta x_{2(i)}|}{|\beta_1 \Delta x_{1(i)}| + |\beta_2 \Delta x_{2(i)}|} * 100\%, \quad (7)$$

where  $\Delta x$  is the difference of current year minus last year. Considering the magnitude of the change, the absolute values of both contributions were calculated, different from Eqs. (2–3).

Note that only ENSO mature winter (DJF) situation was analyzed for such quantification since ENSO mature occurs mostly around the months of DJF based on the previous studies (Wang et al., 2020) and references therein, so ENSO influences on AOD are mostly pronounced in DJF, as discussed in the following Section 5.

### 3 Correlations between different ENSO phases with AOD and AE

The strong correlations between the ENSO phases with AOD were suggested by comparing the composites of anomalous AOD during El Niño and La Niña events, as shown in Fig. 4. The anomalous El Niño month composites (in Figs. 4(a), 4(c) and 4(e)) represent the differences of AOD between El Niño months and non-El Niño months (including both La Niña and Neutral), while the anomalous La Niña month composites (in Figs. 4(b), 4(d) and 4(f)) represent the differences of AOD between La Niña months and non-La Niña months (including both El Niño and Neutral). The difference between El Niño and La Niña has been examined across three different stages of ENSO development from developing (SON), to maturity (DJF), and eventually decay (MAM). In general, AOD reduces during the El Niño period but increases in La Niña period. In particular, with ENSO from the developing autumn to the mature winter process, the difference gradually starts to crop up between El Niño (Fig. 4(c)) and La Niña (Fig. 4(d)), resulting in a reduced AOD (area averages) by 0.097 in El Niño and an increased AOD by 0.029 in La Niña. Such influences from ENSO last until the following state decaying phase (next spring), as shown in Fig. 4(e) (El Niño) and Fig. 4(f) (La Niña) which presents the similar change of AOD as those in the mature period. Clearly, such results demonstrate that the El Niño would result in reduced AOD and improve air quality, while La Niña events would lead to an approximately opposite AOD anomalies and worsen air quality.

The opposite impacts of ENSO on AOD would be explained by its modulation on atmospheric circulation. To demonstrate that, composite anomalous Angstrom Expo-

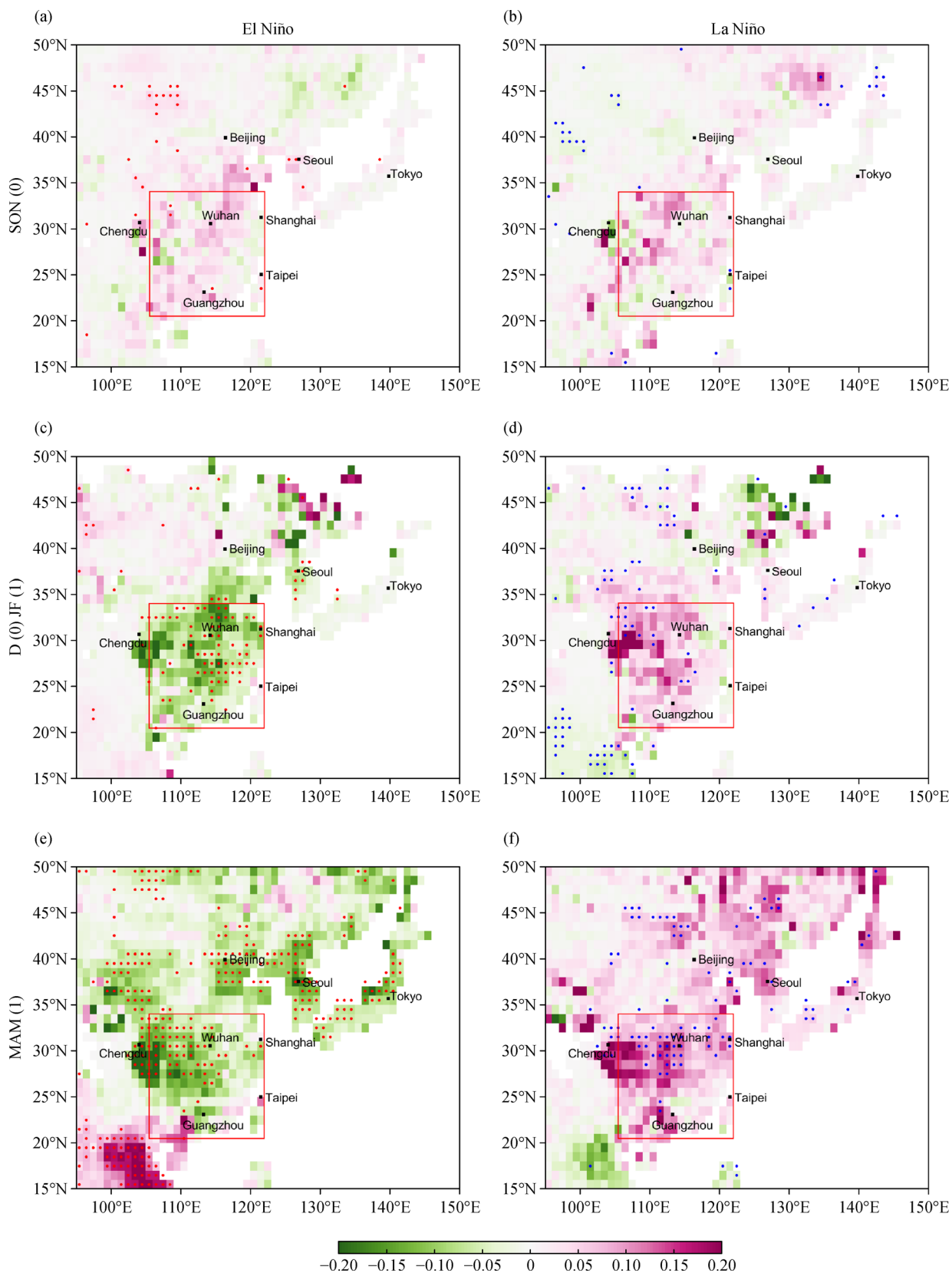


**Fig. 4** Composite AOD anomalies (color shading) in southern region of China during the development period for the El Niño (a, c, e) and the La Niña event (b, d, f). (a) and (b) for the autumn (SON) developing period, (c) and (d) for the winter (DJF) peak period. (e) and (f) for the following (MAM) decaying period. Dots indicate values significantly above the 95% confidence level. AOD = aerosol optical depth. (the 0 represents the previous year, while the 1 represents the current year).

ment (AE, which can be used to indicate the aerosol particle size (Schuster et al., 2006)) were compared between during El Niño and La Niña episodes, as shown in Fig. 5. From the developing autumn to the mature winter process, the AE in El Niño is decreasing (larger aerosol particle size) at the southern part of China, indicating the enhanced contributions from natural aerosols (e.g., sea salts). In contrast, the AE in La Niña is increasing (smaller aerosol particle size) at the southern part of China, suggesting the enhanced contributions from anthropogenic sources. Such phenomenon becomes more significant from winter El Niño mature to springtime decaying period, resulting in lower AE during El Niño (Figs. 5c and 5e) and higher AE during La Niña (Figs. 5d and 5f) across the southern China. Such changes in AE also imply that ENSO phases can impact the spatial distributions of AOD through the modulation of atmospheric circulation.

#### 4 Possible dynamics analysis from ENSO impacts

The variations of ENSO-induced atmospheric circulation was further investigated to understand the potential dynamic mechanism of ENSO effect on the aerosol distribution of Southern China. The anomalous precipitation, humidity, near-surface wind, and 850hpa wind was compared between El Niño and La Niña events in Figs. 6 and 7 and Figs. S3–S5, to explore two mechanisms which are the removal of aerosols (wet deposition) and the regional transport from the north polluted region.

First, the ENSO can significantly modulate precipitation. In general, El Niño brings in abundant rainfall that wash out aerosol particle, resulting in low AOD. The opposing situation is found during La Niña which reduces the precipitation and thus worsens aerosol pollution. From autumn developing to winter mature, the precipitation increased by 0.717 mm/day during El Niño (Figs. 6(a)–6(c)), and decreased by 0.724 mm/day during La Niña (Figs. 6(b)–6(d)). The modulated changes of precipitation last to the decaying period, as the precipitation keeps increasing by 0.228 mm/day during El Niño (Fig. 6(e)), while decreasing by 0.531 mm/day during La Niña (Fig. 6(f)). The surface relative humidity was also modulated during the ENSO events, as displayed in Fig. S3. The relative humidity increased during El Niño. Such wet conditions (Figs. S3c and S3e) are conducive to aerosol hygroscopic growth resulting in large aerosol particles (Figs. 5(c) and 5(e)). In contrast, the relative humidity decreased during La Niña period. Such dry atmosphere (Fig. S3d and S3f) is unfavorable for aerosol hygroscopic growth, resulting in small particle sizes (Figs. 5(d) and 5(f)). The results are also consistent with our finding about the change of AE in previous section.

Second, two ENSO phases have totally different atmospheric teleconnections over the western North

Pacific (WNP) which is the key bridge connecting East tropical Pacific Ocean and East Asia, resulting in the variation of wind fields in Southern China.

For the near-surface (10 m) wind field anomalies (Fig. S4), anomalous anticyclonic circulation appears in WNP (Fig. S4a) in the El Niño developing period (SON). On the other hand, the opposite pattern of anomalous cyclonic circulation appears in the La Niña event (Fig. S4b). During the mature phase of El Niño event (DJF), anticyclone is enhanced significantly, resulting in strong southerly wind (Fig. S4c) and weakens the climatologically winter northerly near surface wind. In contrast, anomalous cyclonic patterns during La Niña occur in WNP, producing northerly anomalies (Fig. S4d) and thus strengthening the climatologically winter northerly wind fields. After the peak period, southerly anomalies and northerly winds are maintained in the springtime decay phase (Figs. S4e and S4f). In addition, sea salt aerosol particles are transported to South China from the ocean by anomalous enhancement of southerly wind. Such imported large sea salt particles are also associated with relatively low AE values during El Niño as shown in Figs. 5(c) and 5(e). On the other hand, anomalous northerly wind brings about anthropogenic aerosol from northern cities to southern China. Such anthropogenic small particles may also explain the relatively high AE values during La Niña events (Figs. 5(d) and 5(f)).

Similar finding was also suggested from the wind field anomalies at the lower troposphere (850 hPa) (Fig. 7), implying that the ENSO also influences large vertical structure of atmosphere. In the developing period of the El Niño, anomalous anticyclonic patterns appear in the WNP (Fig. 7(a)), indicating that strong Philippine anticyclone prevails over the WNP and enhances southerly wind. On the contrary, La Niña period presents the opposite pattern of anomalous cyclonic circulation (Fig. 7(b)). As El Niño (La Niña) enhances, anticyclonic (cyclonic) patterns gets strengthened simultaneously (Figs. 7(c) and 7(d)). Anticyclonic (cyclonic) pattern results in southerly (northerly) anomalies, which weakens (strengthens) climatologically East Asia Winter Monsoon (EAWM). These anomalous patterns are maintained until following springtime decay phase when southerly and northerly wind dominates over South China Sea and parts of Southern China (Figs. 7(e) and 7(f)). This is consistent with previous studies (Wang et al., 2000) which argued that the anomalous WNP wind fields develop rapidly in late autumn of the year with the occurrence of a strong El Niño or La Niña episode matures.

The changes of wind fields associated with the ENSO events are also suggested from the change of geopotential heights in the middle troposphere (500 hPa) (Fig. S5). During ENSO developing phase, anomalous geopotential heights are not obvious (Figs. S5a and S5b). However, extremely high geopotential heights occur during El Niño winter peak period (Fig. S5c), leading to weakened East Asia trough (EAT) which resulted in lesser cold air being

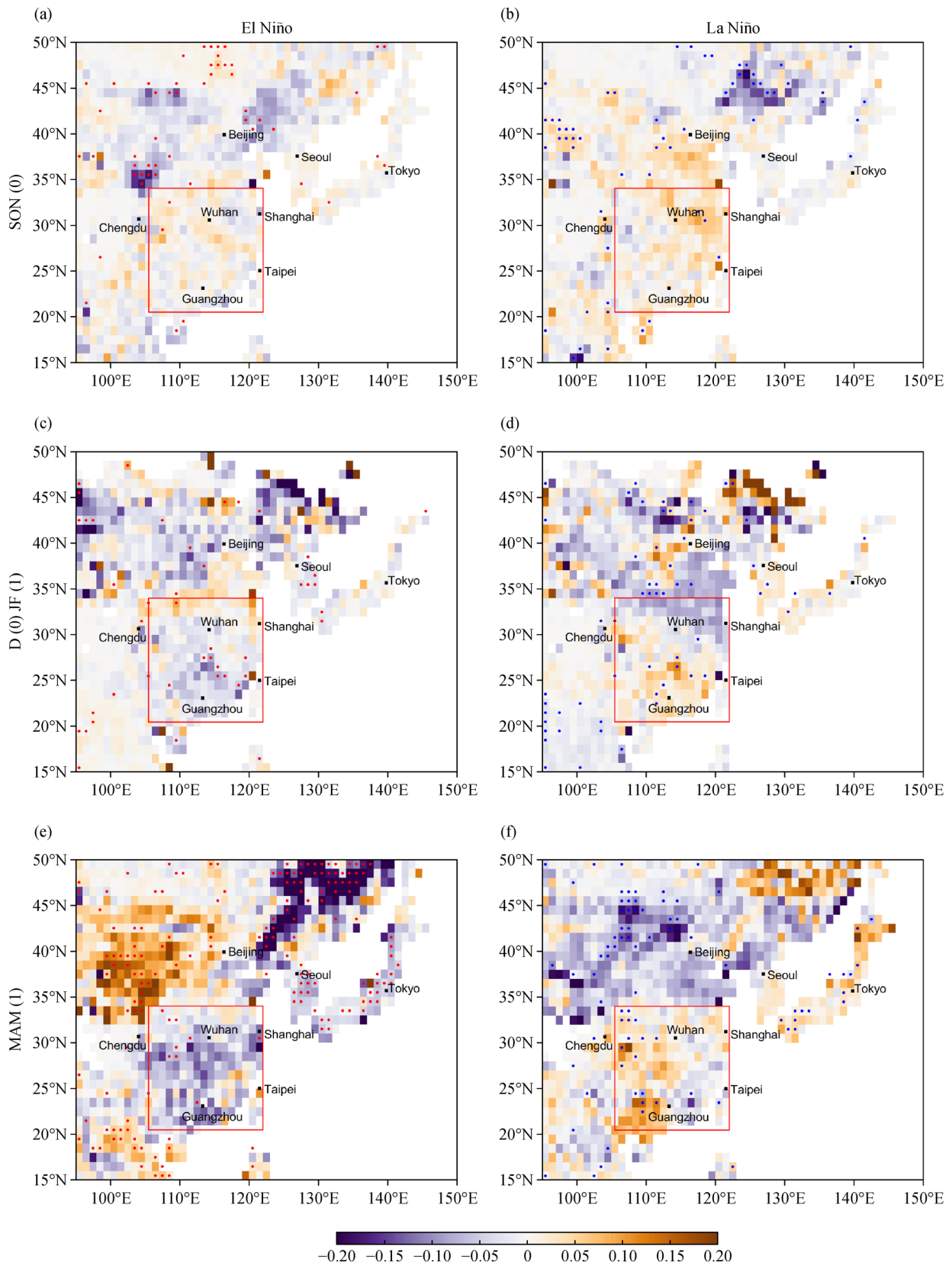


**Fig. 5** Same as Fig. 4, except for composite AE anomalies. AE = Angstrom exponent. Dots indicate AE anomalies that exceeded the 95% confidence level.

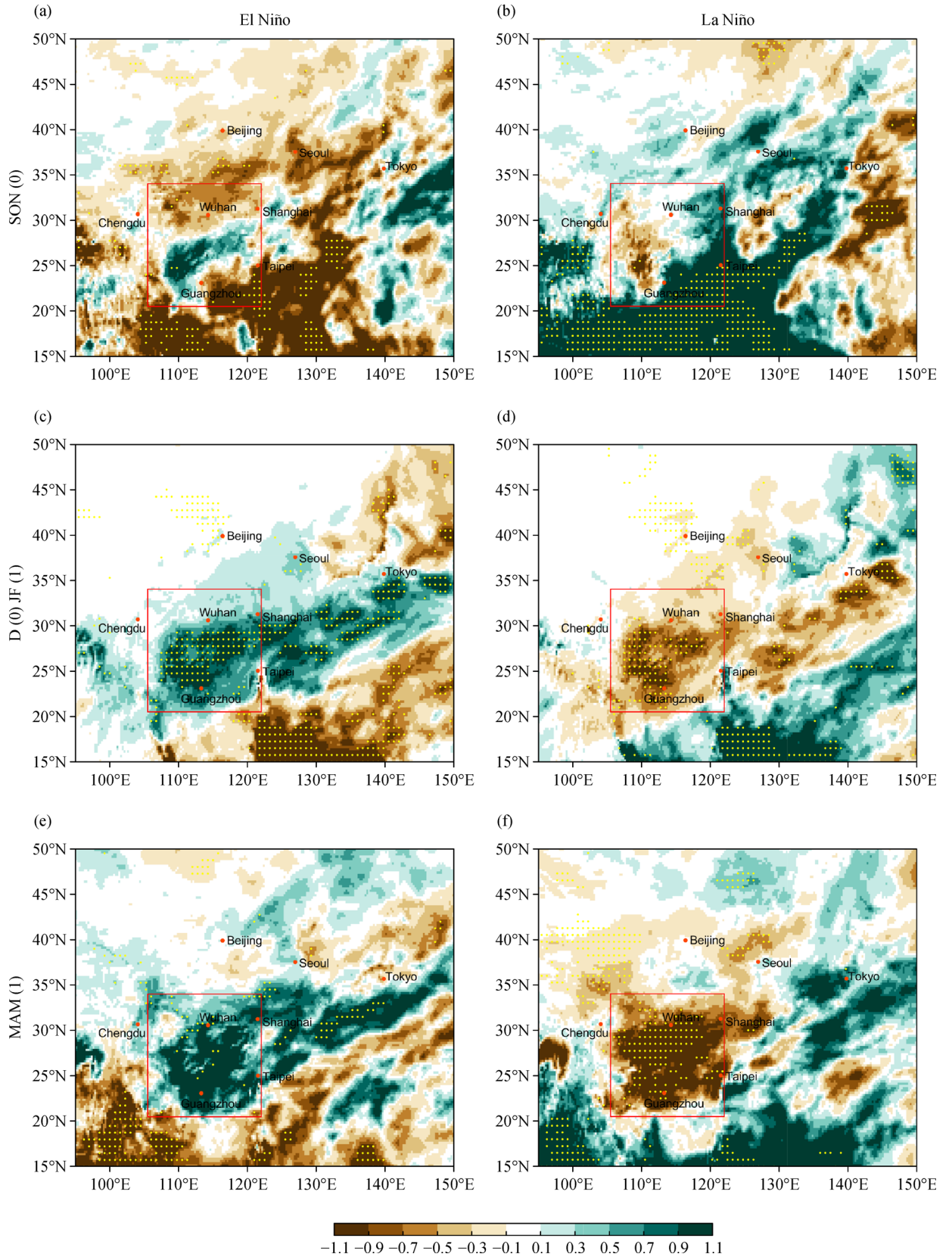


**Fig. 6** Same as Fig. 4, except for composite spatial patterns of anomalous precipitation (mm/day). Dots indicate precipitation anomalies that exceed the 95% confidence level.

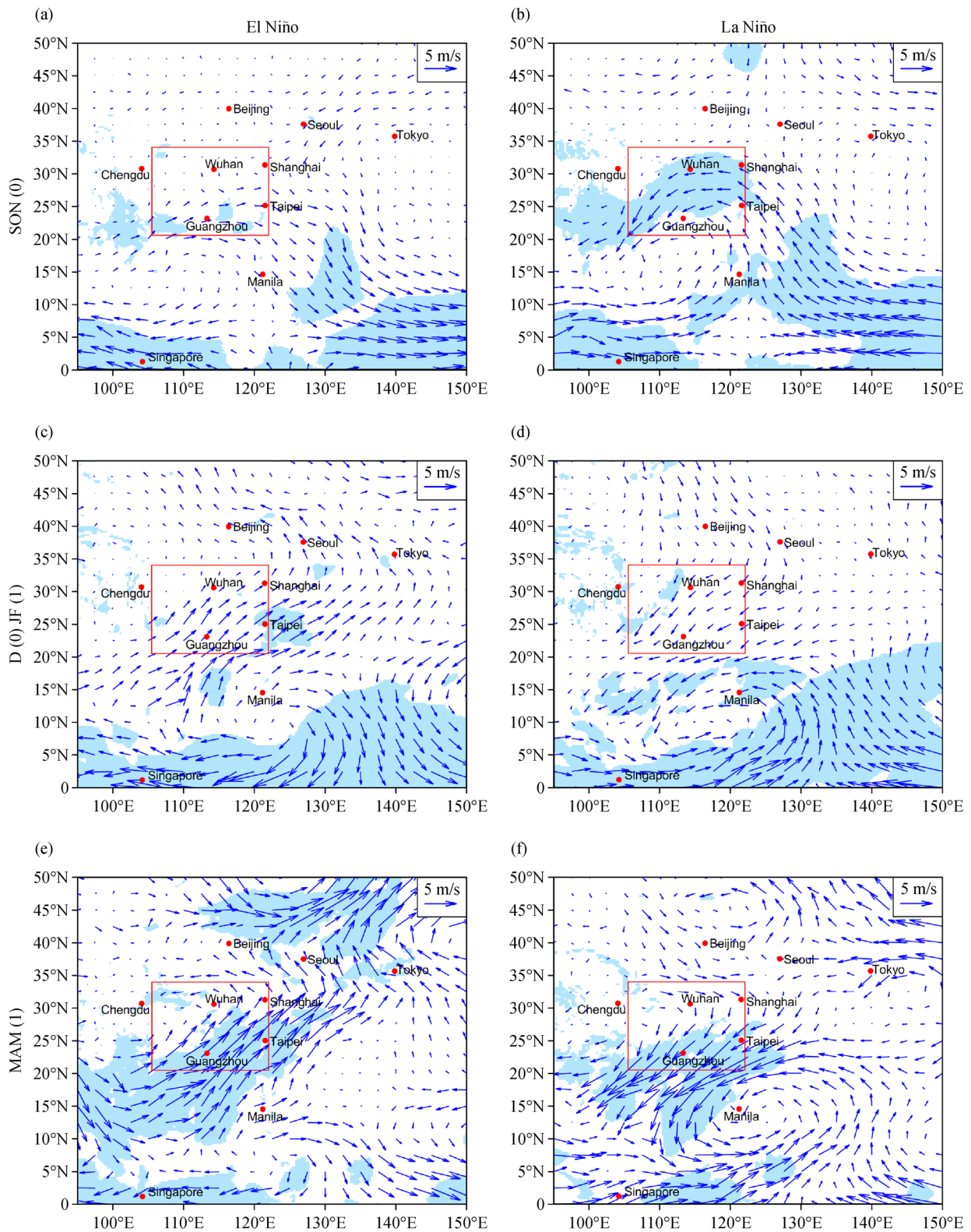


**Fig. 7** Same as Fig. 4, except for 850-hPa wind anomalies composite. Blue shading color represents wind anomalies in m/s above the 95% confidence level.

transported from Siberia to the southern region and thus weakening the EAWM. On the contrary, low geopotential heights (Fig. S5d) will strengthen EAT, and EAWM. This condition is maintained in the following spring, with positive geopotential heights anomalies in El Niño (Fig. S5e) and negative geopotential heights anomalies in La Niña (Fig. S5f).

In summary, El Niño induced anomalous enhanced precipitation and southerly anomalies while it weakened EAT, resulting in a weakened EAWM, while opposite findings are suggested during La Niña event.

## 5 The relative contribution of anthropogenic and natural factors on AOD variations

Previous discussions are mainly focused on the natural influences on AOD based on the averages of 2002–2020. However, the variations of AOD in past two decades are also driven by anthropogenic factors (Liu et al., 2015), particularly after 2013 when China took serious control actions in reducing the emissions (Ding et al., 2019a). To distinguish between the impact of natural (i.e., ENSO in this study) and anthropogenic factors (i.e., emission changes), here we conducted the MLR analysis by quantifying the relative contribution of the changes in emission index and ENSO index to the AOD variations during 2002–2020, as described in method section. The result of Eq. (1) is showed as follows.

$$\begin{aligned} \text{Regress}_{AOD} = & -0.0351 + 0.0802 * x_{\text{emission}} \\ & - 0.0657 * x_{\text{ENSO}}. \end{aligned} \quad (8)$$

The accuracy of MLR equation fitting is  $R$ -Squared ( $R^2$ ) equals 0.545, indicate that more than half of decadal trend of AOD can be explained by the change of anthropogenic emissions and ONI. The relative weight analysis approach was applied to determine the relative importance of variable. We aim to partition explained variance in terms of multiple variates to distinguish individual contributions. Specifically,  $R^2$  equals 0.545 can be attributed to two factors, emission and ENSO contribution. The results indicate a dominant effect of emission, because the raw relative importance of emission is 0.359, which accounts for approximately 65.9% as evaluated from Eq. (1), compared to a secondary effect of ENSO, whose raw relative importance is 0.186 and accounts for 34.1% approximately.

According to the results of Eqs. (2)–(5), during the 18 years from 2002 to 2020, emission accounts for 64.2% while ENSO accounts for 35.8% of total AOD variation. Such result implies that the emission changes are relatively more important than ENSO which drove the decadal trend of AOD.

The time series of anomaly AOD and associated

contributors by ENSO and emission are shown in Fig. 8(a). Before 2014, the increased emissions caused positive anomaly of AOD, indicating uncontrolled emission exacerbated air pollution. However, after 2013 Clean Air Action policy, pollution declined continuously due to the controlled emission. Meanwhile, the impacts of ENSO will either enhance or weaken the effects across the period, as ENSO increases AOD during La Niña episodes while reduces AOD during El Niño events, which is consistent with our discussion in Section 3.

We found that AOD in southern China decreased by as much as 22.4% compared with the climatological mean value (AOD equals 0.479) during the winter of 2015–2016 El Niño (AOD equals 0.372). In addition to emission reduction, the winter super El Niño dominated China's climate and brought in increased precipitation and decreased wind speed (Chang et al., 2016) resulted in less winter haze events in the southern China. In addition, atmospheric circulation in winter 2017 La Niña as well as in winter 2008/2009 with super La Niña was unfavorable for precipitation (Gao and Yang, 2009), and thus resulted in slightly increased AOD.

Variations in anthropogenic emissions dominated the increase in winter AOD over southern China in the long term period, however, in short-term such as year-to-year variations results are quite different, as displayed on Fig. 8(b). We can clearly see that compared with anthropogenic emissions, natural ENSO fluctuation presents greater influence than emissions. On average, ENSO presents a dominant contribution of 70.5% of yearly AOD variations while emission accounts for 29.5% through Eqs. (6) and (7). That implies the stronger influences of ENSO on AOD variation in the short term (annual) period than long-term (decadal) when the emissions are varying significantly like in China.

There are also some limitations about this study. We only use the ONI to represent the level of ENSO phase which seems somehow risky in the regression analysis, however, ENSO does not represent all meteorological elements, including local meteorological changes and fluctuations that are not considered in the MLR model. For example, residual analysis results suggest that the correlation coefficient of surface temperature with AOD is  $-0.3804$ , and the correlation coefficient of boundary layer height (BLH) with AOD is  $0.3042$ , indicating that the change of local temperature and BLH might also explain the changes of AOD to some extent, which were not included in the regression. Meanwhile, the uncertainties about the emissions might also contribute to the biases. Nevertheless, this study conducted long-term analysis of correlations between ENSO and AOD, and demonstrates the importance of ENSO phase in air quality in Southern China. Future studies can be done by considering the different types of ENSO events such as the new type El Niño which has become frequently with climate change (Yeh et al., 2009; Lee and Mcphaden, 2010) and other

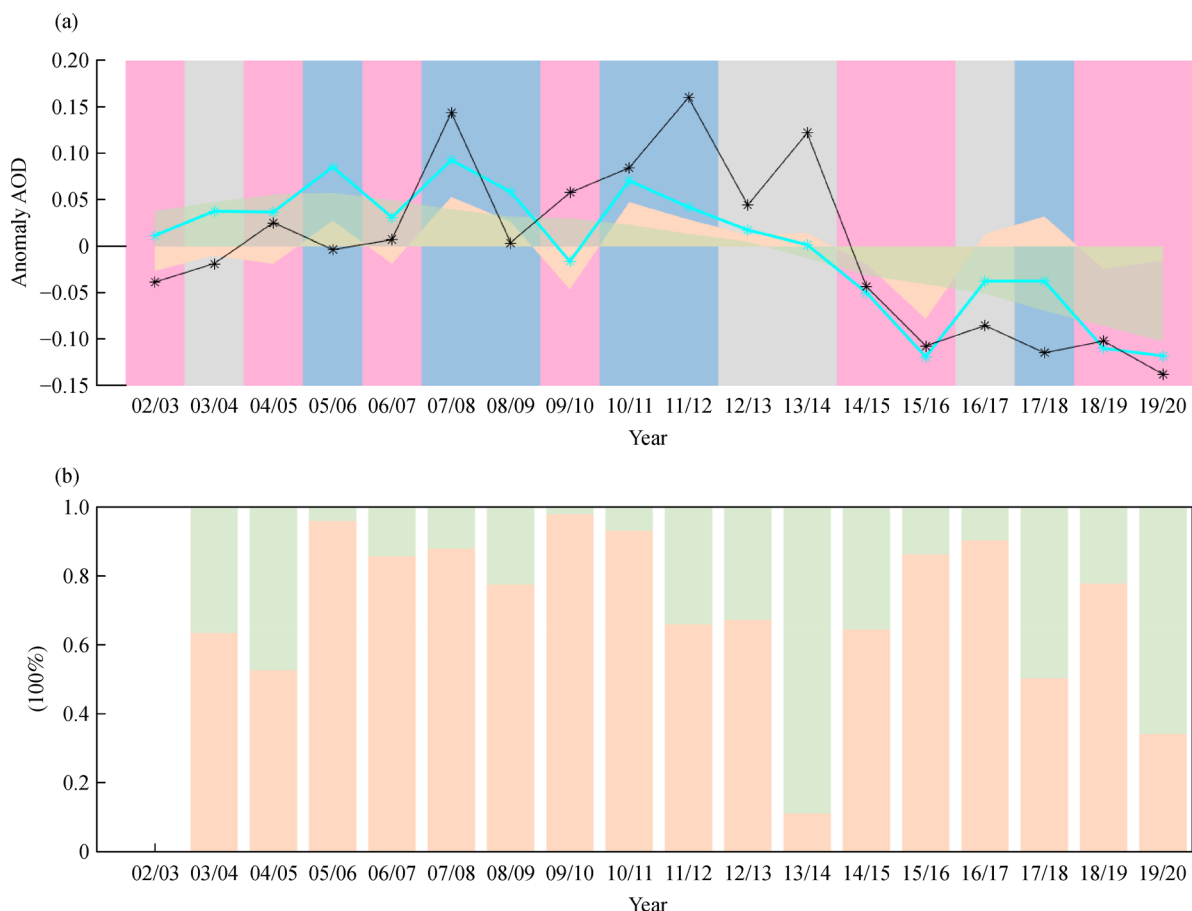


**Fig. 8** (a) The winter (DJF) AOD variation caused by emission and ENSO respectively. Black line is the anomaly value of AOD value (observed value), gray dash line is value equals to zero. Cyan line is the sum of emission and ENSO (fitted value). Green shade shows AOD change caused by emissions and orange shade caused by ENSO events. Red, blue, and gray color bar represents El Niño, La Niña event and Neutral, respectively. (b) The annual AOD variation attributed to emission (green) and ENSO (orange). Y axis is percentage.

climate phenomena, such as from high-latitude signal which could also exert influence on aerosol distribution.

Though our analysis focused on the impacts of ENSO events on the southern region, the ENSO influence extends to a much greater space (Yu et al., 2020). For example, ENSO caused accumulation of aerosol pollutants which increased in winter during canonical El Niño called eastern Pacific (EP) El Niño, while aerosol pollutants decreased in winter due to a new type of El Niño called central Pacific (CP) El Niño events (Yu et al., 2020). It is noteworthy that the potential effect of ENSO would be greater in terms of its spatial range, and more variable along with the future climate change.

## 6 Conclusions

ENSO, as a large-scale ocean-atmosphere interaction originating from the tropical Pacific Ocean, has a significant modulation on the air quality over southern China. In this study, we investigated the correlations

between aerosol loading properties and the ENSO development phase in Southern China. Results suggest that the aerosol anomaly patterns were roughly opposite during El Niño and La Niña episodes in Southern China, with cleaner air quality during El Niño period but worse air quality during La Niña period. Low AOD occurs in El Niño but high AOD occurs in La Niña events in southern China. The possible reason includes the ENSO-induced precipitation anomalies and wind fields. El Niño resulted in higher precipitation (wet scavenging) over southern China that conduces to decrease in aerosol. In contrast, La Niña results in an opposite situation, less precipitation resulting in more severe air pollution. In addition, anomalous positive AE during La Niña period suggested that relative high AE values were characterized by the abundance of fine-mode aerosol particles due to the enhancement of EAWM, likely attributed by northern anthropogenic city activities. On the other hand, the influx of sea salt aerosol particles to South China from the ocean by anomalous enhancement of southerly wind is likely associated with the relatively low AE values during El Niño. We further quantified the relative importance of anthropogenic

emission and ENSO to the AOD variation. Results suggest that during 2002–2020, change of anthropogenic emissions is the dominant driver (64.2%) for the AOD in long-term decadal trend, while ENSO exerts large influence (70.5%) on annual variations of AOD. So, our conclusion is the change of anthropogenic emissions dominate the long-term (decadal) variations of aerosol concentration, while ENSO events dominate the short-term (yearly) AOD variation.

**Acknowledgements** This research was funded by the Foundation for Innovative Research Groups of the Hubei Natural Science Foundation, grant number 2020CFA003 and the National Natural Science Foundation of China, grant number 41975022. The authors are grateful to NOAA CPC for ONI-3.4 index data, LAADS DAAC for Aqua MODIS AOD data, and ECMWF for sharing the reanalysis data publicly accessible.

**Electronic Supplementary Material** Supplementary material is available in the online version of this article at <https://doi.org/10.1007/s11783-021-1460-0> and is accessible for authorized users.

## References

- Cai W, Li K, Liao H, Wang H, Wu L (2017). Weather conditions conducive to Beijing severe haze more frequent under climate change. *Nature Climate Change*, 7(4): 257–262
- Cai W, Wang G, Dewitte B, Wu L, Santoso A, Takahashi K, Yang Y, Carréric A, McPhaden M J (2018). Increased variability of eastern Pacific El Niño under greenhouse warming. *Nature*, 564(7735): 201–206
- Capotondi A (2015). Extreme La Niña events to increase. *Nature Climate Change*, 5(2): 100–101
- Chang L, Xu J, Tie X, Wu J (2016). Impact of the 2015 El Niño event on winter air quality in China. *Scientific Reports*, 6(1): 34275
- Chen Z, Wu R, Chen W (2014). Distinguishing interannual variations of the northern and southern modes of the East Asian winter monsoon. *Journal of Climate*, 27(2): 835–851
- Ding D, Xing J, Wang S, Chang X, Hao J (2019b). Impacts of emissions and meteorological changes on China's ozone pollution in the warm seasons of 2013 and 2017. *Frontiers of Environmental Science & Engineering*, 13(5): 76
- Ding D, Xing J, Wang S, Liu K, Hao J (2019a). Estimated contributions of emissions controls, meteorological factors, population growth, and changes in baseline mortality to reductions in ambient PM<sub>2.5</sub> and PM<sub>2.5</sub>-related mortality in China, 2013–2017. *Environmental Health Perspectives*, 127(6): 67009
- Ding Y, Wu P, Liu Y, Song Y (2017). Environmental and dynamic conditions for the occurrence of persistent haze events in North China. *Engineering*, 3(2): 266–271
- Feng J, Li J, Zhu J, Liao H (2016). Influences of El Niño Modoki event 1994/1995 on aerosol concentrations over southern China. *Journal of Geophysical Research: Atmospheres*, 121(4): 1637–1651
- Feng J, Li J, Zhu J, Liao H, Yang Y (2017). Simulated contrasting influences of two La Niña Modoki events on aerosol concentrations over eastern China. *Journal of Geophysical Research: Atmospheres*, 122(5): 2734–2749
- Gao H, Yang S (2009). A severe drought event in Northern China in winter 2008–2009 and the possible influences of La Niña and Tibetan Plateau. *Journal of Geophysical Research: Atmospheres*, 114(D24): D24104
- Jiang Y, Xing J, Wang S, Chang X, Liu S, Shi A, Sahu S K (2021). Understand the local and regional contributions on air pollution from the view of human health impacts. *Frontiers of Environmental Science & Engineering*, 15(5): 11
- Kim S, Yoon S, Kim J, Kim S (2007). Seasonal and monthly variations of columnar aerosol optical properties over East Asia determined from multi-year MODIS, LIDAR, and AERONET sun/sky radiometer measurements. *Atmospheric Environment*, 41(8): 1634–1651
- Koren I, Altaratz O, Remer L A, Feingold G, Martins J V, Heiblum R H (2012). Aerosol-induced intensification of rain from the tropics to the mid-latitudes. *Nature Geoscience*, 5(2): 118–122
- Lee T, McPhaden M J (2010). Increasing intensity of El Niño in the central-equatorial Pacific. *Geophysical Research Letters*, 37(14): L14603: n/a
- Liu T, Gong S, He J, Yu M, Wang Q, Li H, Liu W, Zhang J, Li L, Wang X, Li S, Lu Y, Du H, Wang Y, Zhou C, Liu H, Zhao Q (2017). Attributions of meteorological and emission factors to the 2015 winter severe haze pollution episodes in China's Jing-Jin-Ji area. *Atmospheric Chemistry and Physics*, 17(4): 2971–2980
- Liu Z, Guan D, Wei W, Davis S J, Ciais P, Bai J, Peng S, Zhang Q, Hubacek K, Marland G, Andres R J, Crawford-Brown D, Lin J, Zhao H, Hong C, Boden T A, Feng K, Peters G P, Xi F, Liu J, Li Y, Zhao Y, Zeng N, He K (2015). Reduced carbon emission estimates from fossil fuel combustion and cement production in China. *Nature*, 524(7565): 335–338
- Ma T, Duan F, He K, Qin Y, Tong D, Geng G, Liu X, Li H, Yang S, Ye S, Xu B, Zhang Q, Ma Y (2019). Air pollution characteristics and their relationship with emissions and meteorology in the Yangtze River Delta region during 2014–2016. *Journal of Environmental Sciences*, 83: 8–20
- Ramon J, Lledo L, Torralba V, Soret A, Doblas-Reyes F J (2019). What global reanalysis best represents near-surface winds? *Quarterly Journal of the Royal Meteorological Society*, 145(724): 3236–3251
- Shang D, Peng J, Guo S, Wu Z, Hu M. (2021). Secondary aerosol formation in winter haze over the Beijing-Tianjin-Hebei Region, China. *Frontiers of Environmental Science & Engineering*, 15(2): 13
- Schuster G L, Dubovik O, Holben B N (2006). Angstrom exponent and bimodal aerosol size distributions. *Journal of Geophysical Research-Atmospheres*, 111(D07207D7)
- Sun J, Li H, Zhang W, Li T, Zhao W, Zuo Z, Guo S, Wu D, Fan S (2018). Modulation of the ENSO on winter aerosol pollution in the eastern region of China. *Journal of Geophysical Research: Atmospheres*, 123(21): 11952–11969
- Tai A P K, Mickley L J, Jacob D J (2010). Correlations between fine particulate matter (PM<sub>2.5</sub>) and meteorological variables in the United States: Implications for the sensitivity of PM<sub>2.5</sub> to climate change. *Atmospheric Environment*, 44(32): 3976–3984
- Wang B, Luo X, Liu J (2020). How robust is the Asian precipitation-ENSO relationship during the industrial warming period (1901–2017)? *Journal of Climate*, 33(7): 2779–2792
- Wang B, Wu R G, Fu X H (2000). Pacific-East Asian teleconnection: How does ENSO affect East Asian climate? *Journal of Climate*, 13

- (9): 1517–1536
- Wang X, Zhong S, Bian X, Yu L (2019). Impact of 2015–2016 El Niño and 2017–2018 La Niña on PM<sub>2.5</sub> concentrations across China. *Atmospheric Environment*, 208: 61–73
- Wu X, Xu Y, Kumar R, Barth M (2019). Separating emission and meteorological drivers of mid-21<sup>st</sup>-century air quality changes in India based on multiyear global-regional chemistry-climate simulations. *Journal of Geophysical Research: Atmospheres*, 124(23): 13420–13438
- Xing J, Lu X, Wang S, Wang T, Ding D, Yu S, Shindell D, Ou Y, Morawska L, Li S, Ren L, Zhang Y, Loughlin D, Zheng H, Zhao B, Liu S, Smith K R, Hao J (2020a). The quest for improved air quality may push China to continue its CO<sub>2</sub> reduction beyond the Paris Commitment. *Proceedings of the National Academy of Sciences of the United States of America*, 117(47): 29535–29542
- Xing J, Zheng S, Ding D, Kelly J T, Wang S, Li S, Qin T, Ma M, Dong Z, Jang C, Zhu Y, Zheng H, Ren L, Liu T Y, Hao J (2020b). Deep learning for prediction of the air quality response to emission changes. *Environmental Science & Technology*, 54(14): 8589–8600
- Yeh S W, Kug J S, Dewitte B, Kwon M H, Kirtman B P, Jin F F (2009). El Niño in a changing climate. *Nature*, 461(7263): 511–514
- Yin Z, Wang H, Chen H (2017). Understanding severe winter haze events in the North China Plain in 2014: Roles of climate anomalies. *Atmospheric Chemistry and Physics*, 17(3): 1641–1652
- Yu X, Wang Z, Zhang H, He J, Li Y (2020). Contrasting impacts of two types of El Niño events on winter haze days in China's Jing-Jin-Ji region. *Atmospheric Chemistry and Physics*, 20(17): 10279–10293
- Zhang G, Gao Y, Cai W, Leung L R, Wang S, Zhao B, Wang M, Shan H, Yao X, Gao H (2019). Seesaw haze pollution in North China modulated by the sub-seasonal variability of atmospheric circulation. *Atmospheric Chemistry and Physics*, 19(1): 565–576
- Zhang R H, Li Q, Zhang R N (2014). Meteorological conditions for the persistent severe fog and haze event over Eastern China in January 2013. *Science China. Earth Sciences*, 57(1): 26–35
- Zhao S, Li J, Sun C (2016). Decadal variability in the occurrence of wintertime haze in central Eastern China tied to the Pacific Decadal Oscillation. *Scientific Reports*, 6(1): 27424
- Zhu J, Liao H, Li J (2012). Increases in aerosol concentrations over eastern China due to the decadal-scale weakening of the East Asian summer monsoon. *Geophysical Research Letters*, 39(9 L09809): n/a
- Zou Y, Wang Y, Zhang Y, Koo J H (2017). Arctic sea ice, Eurasia snow, and extreme winter haze in China. *Science Advances*, 3(3): e1602751